Journal of Catalysis 287 (2012) 44–54

Contents lists available at SciVerse ScienceDirect

Journal of Catalysis

journal homepage: www.elsevier.com/locate/jcat

Effect of reduction in liquid phase on the properties and the catalytic activity of Pd/Al_2O_3 catalysts

Elena Groppo [a,*], Giovanni Agostini [a], Andrea Piovano [a,1], Naresh B. Muddada [a,2], Giuseppe Leofanti [b], Riccardo Pellegrini [c], Giuseppe Portale [d], Alessandro Longo [e], Carlo Lamberti [a]

[a] Department of Inorganic, Physical and Materials Chemistry, INSTM Reference Center and NIS Centre of Excellence, Università di Torino, Via P. Giuria 7, I-10125 Torino, Italy
[b] Consultant, Via Firenze 43, 20010 Canegrate (Milano), Italy
[c] Chimet SpA – Catalyst Division, Via di Pescaiola 74, I-52041 Viciomaggio (Arezzo), Italy
[d] Netherlands Organization for Scientific Research at ESRF, BP 220, F-38043 Grenoble Cedex 9, France
[e] Istituto per lo Studio dei Materiali Nanostrutturati del CNR, Via Ugo La Malfa 153, I-90146 Palermo, Italy

ARTICLE INFO

Article history:
Received 24 August 2011
Revised 11 November 2011
Accepted 30 November 2011
Available online 12 January 2012

Keywords:
Pd-based catalysts
Heterogeneous catalysis
Characterization techniques
Temperature-programmed reduction
FT-IR spectroscopy
CO chemisorption
TEM
X-ray absorption spectroscopy
SAXS

ABSTRACT

The change in structural and surface properties of Pd/Al_2O_3 catalysts as the effect of reduction in liquid phase during preparation is investigated by a multi-technical approach. It has been found that, although the treatment leaves an external shell of oxidized Pd because of the exposure to air of final wet catalyst, it affects both the catalyst reducibility and the properties of the supported Pd nanoparticles, in terms of dispersion, particle size, morphology, interaction with the support, structural order, and surface properties. Consequently, unreduced and pre-reduced catalysts show different performances in the debenzylation of 4-benzyloxyphenol reaction.

1. Introduction

Pd-supported catalysts are widely used in hydrogenation reactions for the synthesis of fine chemicals (*e.g.*, active pharmaceutical ingredients) [1] and bulk chemicals (*e.g.*, terephthalic acid) [2]. Although Pd catalysts find application for reactions in gas phase [3], more often they are used for reactions in liquid phase [4–7], and thus more conveniently supplied in the wet form, *i.e.*, with pores filled by water. Pd catalysts are usually prepared by supporting a Pd precursor on high surface area carriers, among which metal oxides, such as Al_2O_3 and carbons are the most used. We have recently demonstrated that, whichever is the support, following the deposition–precipitation method, Pd is supported in the form of a Pd-oxide or hydroxide [8]. Depending on the specific catalytic process in which they are used, Pd catalysts can be supplied directly in this oxidized state or can be further reduced by the catalyst manufacturer itself through different reducing agents (among which sodium formate, sodium borohydride, and hydrogen are the most common ones).

Although the active Pd phase in reductive conditions typical of hydrogenation reaction is metal Pd, the oxidation state of the starting catalyst (*i.e.*, unreduced or pre-reduced) influences its catalytic performances in such a way that sometimes it is more convenient to use an unreduced catalyst [9–11], and some others a reduced catalyst shows better performances [12,13]. This suggests that the physical–chemical properties of the supported Pd particles depend on the reduction state and on the reduction method. However, a clear relationship among the reduction state of the catalyst as loaded into the reactor, its physical–chemical properties, and the catalytic performances, was never demonstrated so far.

We will show that the catalytic performances of alumina-supported Pd-based catalysts in the debenzylation of 4-benzyloxyphenol (chosen as test reaction) are influenced by a pre-reduction in liquid phase, in terms of induction time, activity, and turnover

* Corresponding author. Fax: +39 011 6707855.
E-mail address: elena.groppo@unito.it (E. Groppo).
[1] Present address: Institut Laue Langevin, 6 Rue Jules Horowitz BP 156, F-38042 Grenoble Cedex 9, France.
[2] Present address: inGAP Centre of Research-based Innovation, Department of Chemistry, University of Oslo, Sem Saerlandsvei 26, N-0315 Oslo, Norway.

0021-9517/$ - see front matter © 2011 Elsevier Inc. All rights reserved.
doi:10.1016/j.jcat.2011.11.018

frequency. In an attempt to understand the origin of these changes, we performed a systematic investigation of the structural and surface properties of Pd/Al_2O_3 catalysts as a function of the reduction state (unreduced or pre-reduced with different reducing agents). The oxidation state of the supported Pd phase was evaluated by means of TPR, whereas the surface oxidation state was determined by FT-IR spectroscopy of CO adsorbed at 100 K. CO chemisorption, TEM, and SAXS were successively adopted to determine the dispersion and the morphology of the Pd particle. At last, Pd hydride decomposition in TPR experiments and FT-IR of CO adsorbed at room temperature were used to investigate the order/disorder characteristics of bulk and surface Pd particles, as well as the nature of the exposed surface sites. This multi-technical approach, already applied by us to investigate various Pd-supported catalysts [8,14–17], is fundamental to understand the role of pre-reduction in determining the reducibility of supported Pd-oxide or hydroxide and the properties of the final Pd nanoparticles.

2. Experimental

2.1. Catalysts preparation and nomenclature

Supported Pd samples were prepared in the Chimet Laboratories on γ-Al_2O_3 (surface area = 121 $m^2\,g^{-1}$; pore volume = 0.43 $cm^3\,g^{-1}$) following the deposition–precipitation method, with Na_2PdCl_4 as palladium precursor and Na_2CO_3 as basic agent [8]. Three Pd loadings were investigated: 5.0 wt.%, which is relevant for industrial applications, and 2.0 and 3.5 wt.% for comparison. All catalysts were carefully washed until complete Cl^- removal was achieved and were kept in their wet state (*ca.* 50% of water) until measurement. The same procedure was followed to prepare supported Pd samples on a wood-based activated carbon (surface area = 980 $m^2\,g^{-1}$; pore volume = 0.62 $cm^3\,g^{-1}$), which were used for the evaluation of mass transfer phenomena in the catalytic tests. For the 5.0 wt.% catalyst, after the deposition of palladium as hydroxide, reduction was carried out in liquid phase by means of three different reducing agents, i.e., HCOONa, $NaBH_4$, or hydrogen at 338 K. For reduction with hydrogen, the treatment was performed inside a stainless steel autoclave, under 10 bar of pressure. As for unreduced catalysts, the reduced catalysts were successively water-washed until the residual Cl^- was completely removed and stored in their wet state.

Hereafter, the nomenclature PdAl and PdCw are used to indicate the unreduced catalysts prepared on alumina (Al) and wood carbon (Cw), respectively. The Pd loading is indicated before the PdAl label; thus, 5PdAl refers to the 5.0 wt.% loading. When a reduction in the liquid phase is performed, a label indicating the reducing agent is added. Thus, 5PdAl(F), 5PdAl(B), and 5PdAl(H) refer to alumina-supported palladium catalysts (5.0 wt.% loading) reduced with formate, borohydride, and hydrogen, respectively, whereas PdCw(F) refers to carbon-supported palladium catalyst reduced with formate. All the Pd-supported samples were stored in their wet state. TPR data provided evidence that the drying atmosphere greatly affects the reduction temperature of the catalysts: a sample dried in inert atmosphere starts to be reduced at lower temperature than the same sample dried in air. The reason is attributed to the auto-reduction of a very small fraction of defective sites, as demonstrated also by FT-IR spectroscopy of CO adsorbed at 100 K (vide infra) and as already suggested in the literature [18–20]. This observation is relevant in order to avoid misleading comparisons with similar data in literature. However, it was found that all the properties of Pd-supported particles before and after reduction (such as the Pd^{2+}/Pd_{tot} ratio and the Pd dispersion) are not affected by the drying procedure. Therefore, the drying step was always conducted in air (unless specified).

To take into account the possible modification of the γ-Al_2O_3 pore size distribution upon Pd precipitation, a fraction of the γ-Al_2O_3 support was subjected to the deposition–precipitation process without adding the Pd precursor. This sample was used to simulate the contribution of the support in the SAXS experiments. Finally, unsupported PdO sample was prepared as a reference for TPR experiments following a procedure similar to that adopted for the catalysts preparation, but omitting the support. The final unsupported samples were dried overnight in air at 393 K.

2.2. Catalysts activity in debenzylation reaction

The catalytic performance of the Pd/Al_2O_3 samples was tested in the debenzylation of 4-benzyloxyphenol to hydroquinone and toluene. The reaction was carried out in a 300 cm^3 glass reactor equipped with a double mantle for water circulation and a gas injection stirrer (Premex, br1 series). Water at the required temperature was circulated inside the reactor mantle by means of a thermostatic bath. In a typical experiment, the reactor was charged with 500 mg of dry catalyst and then a solution of 10 g of 4-benzyloxyphenol in 140 ml of ethanol was poured into the reactor. The reactor was purged first with nitrogen and then with hydrogen. Hydrogenation was performed at atmospheric pressure, at a temperature of 308 K, and with a stirring speed of 2000 rpm.

By plotting the hydrogen consumption versus time, a straight line is obtained, demonstrating that the reaction has a zero-order with respect to the substrate. The slope of this line corresponds to the activity (hereafter r), expressed in cm^3 STP min^{-1}, and the intercept with the abscissa has been taken as the measure of the induction time. The mean activity of surface Pd atoms can be defined in terms of turnover frequency (TOF), which is the number of H_2 molecules consumed per second per number of surface atoms determined by an independent technique [21], in this work by CO chemisorption.

To prove that the reaction proceeds without mass transfer constraints in the conditions adopted herein, several tests with different catalyst amounts (*i.e.*, 300, 500, and 700 mg), different catalyst particle size (*i.e.*, 5 and 23 μm), and at different temperatures (i.e., 293, 308, and 323 K) were performed [22–24]. The effect of particle size on catalytic activity was evaluated on PdCw(F), having a particle size of 23 μm (measured by LALLS technique with Malvern Mastesizer 2000 instrument). The catalyst particle size was decreased to 5 μm by grinding. CO chemisorption data demonstrated that the grinding procedure does not affect the palladium dispersion. By using a simplified approach [22], the reciprocal plot $1/r$ versus $1/m$ (Fig. 1a) allowed us to calculate the mass transfer coefficient for the transfer of the gas to liquid phase (k_m) and the pseudo-kinetic constant, which includes the mass transport to the solid–liquid interface, as well as internally to the porous solid (k_r). The ratio k_m/k_r resulted in a value higher than 10^3, providing evidence that the transfer of the gas (*i.e.*, H_2) is much quicker than the reaction rate; and this happens at almost the same extent regardless of the catalyst particle size (5 or 23 μm).

The Arrhenius plot shown in Fig. 1b further confirms the abovementioned results, giving an activation energy value equal to 52.3 kJ/mol (12.5 kcal/mol). According to Roberts [24], when a reaction is controlled by either gas/liquid or liquid/solid mass transport, the observed activation energy should be less than 5 kcal/mol, whereas activation energy values greater than 10 kcal/mol (as in our case) are an indication that the reaction proceeds without mass transfer constraints, either with or without pore diffusion. Moreover, the fact that the reciprocal plot of Fig. 1a is the same for both catalysts having a different particle size (*i.e.*, 5 and 23 μm) provides evidence that the reaction rate depends only on the chemical reaction taking place on active Pd sites, without the influence of internal pore diffusion [23].

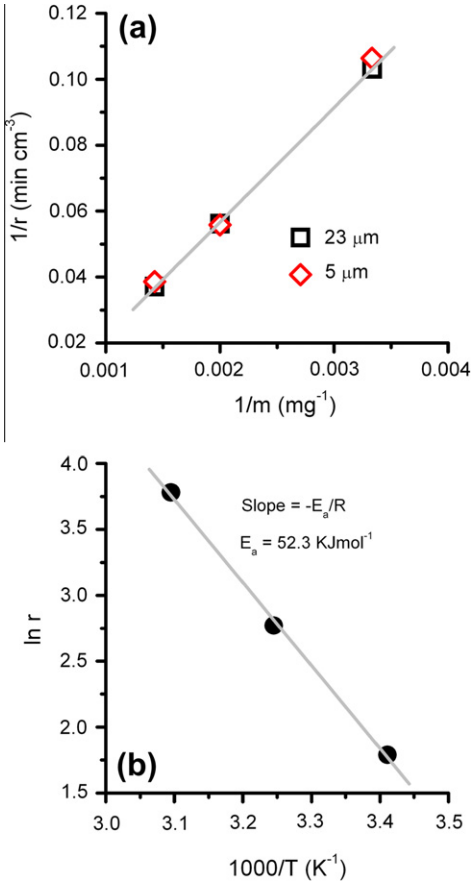

Fig. 1. Mass transfer evaluation in the debenzylation of 4-benzyloxyphenol. Part (a): reciprocal plot of activity (r) versus the catalyst amount (m). Reaction conditions: PdCw(F) catalyst, atmospheric pressure, 308 K, 2000 rpm stirring speed, catalyst loading: 300, 500, and 700 mg. Part (b): Arrhenius plot. PdCw(F) catalyst, atmospheric pressure, catalyst loading 500 mg, 2000 rpm stirring speed, temperature: 293, 308, and 323 K.

2.3. Catalysts characterization

2.3.1. Temperature-Programmed Reduction (TPR) and CO Chemisorption

A Micromeritics Autochem 2910 instrument was used for both, TPR and CO chemisorption measurements. For the TPR measurements, the instrument was equipped with a CryoCooler device allowing to perform the measurements starting from 153 K. The water formed during the reduction process was trapped inside a molecular sieve getter located between the sample holder and the detector. A typical procedure was as follows: 100 mg of sample (either wet or dry) is introduced in the sample holder and, when necessary, heated *in situ* by a nitrogen flow at 393 K for 2 h [8,15]. Then, the sample is cooled down to 153 K under Ar flow (50 cm^3 min^{-1}). Successively, the flow is switched to 5% H_2 in Ar (50 cm^3 min^{-1}) and maintained throughout the analysis. Once a baseline is established, the temperature ramp is started at a rate of 5 K min^{-1} up to 623 K. T_{max} and T_{min} indicate the temperatures of the maximum rate of H_2 consumption or release, respectively. T_{start} is the temperature of the beginning of H_2 consumption, defined as the temperature where the first derivative of the TCD signal versus temperature exceeds the arbitrary value of 5×10^{-4}. Note that all the TPR curves shown hereafter present a minimum around 230 K, which is an instrumental artefact due to a small change in the heating rate.

CO chemisorption measurements were performed at 323 K by a dynamic pulse method on samples pre-reduced in H_2 at 393 K [25]. In a typical experiment, the catalyst (200 mg) was reduced *in situ* at 393 K according to the following procedure: (i) the catalyst is loaded inside the U-tube, (ii) it is heated in He up to 393 K (ramp rate of 10 K min^{-1}), (iii) H_2 is fed for 30 min, and (iv) the sample is cooled down to 323 K in He (ramp rate of 10 K min^{-1}). A CO/Pd average stoichiometry = 1 was assumed to calculate the Pd dispersion. This assumption was verified by measurements performed simultaneously in a static volumetric apparatus on three samples reduced at two different temperatures (393 and 673 K) using both, H_2 and O_2 as probe molecules; these measurements gave a O/Pd average stoichiometry close to 1 [14,26]. Comparing the results obtained according to the two methods, a CO/O ratio in the 0.94–1.13 range was obtained, which is a strong support for a CO/Pd average stoichiometry = 1.

2.3.2. Transmission Electron Microscopy (TEM)

Transmission electron micrographs were obtained using a JEOL 3010-UHR instrument operating at 300 kV, equipped with a 2 k × 2 k pixels Gatan US1000 CCD camera. Samples were deposited on a copper grid covered with a lacey carbon film.

2.3.3. Small-Angle X-ray Scattering (SAXS)

SAXS measurements were taken at the synchrotron DUBBLE beamline BM26B [27] at the European Synchrotron Radiation Facilities (ESRF, Grenoble, F). Experiments were carried out using a monochromatic 12 keV X-ray beam. The H-hutch of BM26B is equipped to perform SAXS/WAXS experiments and was designed with a maximum of flexibility that allows one to study several problems, particularly in the field of nanoscience [27]. In our experiments, the small-angle scattering images were recorded by placing a two-dimensional PilatusPilatus 1 M detector (by Dectris) at 6 m. Thus, a large scattering vector range was covered, $0.1 < q < 3.5$ nm^{-1} (being q [nm^{-1}] = $10 \times 1.014E$ [19] $\sin\theta$ the scattering vector, where θ is the scattering angle and E is the energy of the X-ray beam) and the maximum d-spacing resolution was 62.8 nm. Silver Behenate was used as standard to determine the centre of the beam and the scattering vector scale. Then, the isotropic SAXS intensity profiles were obtained by the integration of the two-dimensional images radially averaged around the centre of the primary beam by using FIT2D software [28–30]. The analysis details will be described in a forthcoming paper.

2.3.4. FT-IR spectroscopy of adsorbed CO

The FT-IR spectra of CO adsorbed on the catalysts were recorded at a resolution of 2 cm^{-1} on a Bruker Vertex 70 instrument, in transmission mode. *In situ* experiments were carried out in a homemade quartz cell equipped with KBr windows allowing to perform sample activation and successive measurements in the 100–823 K temperature range, at pressures from 10^{-4} to 760 Torr. The catalysts were pressed into self-supporting pellets and activated in the same cells used for the measurement. Both activation and measurements were performed using grease-free cells and vacuum lines.

A first set of experiments was aimed to determine the surface oxidation state of the Pd phase on the fresh samples. For this reason, the samples were heated at 393 K in air, followed by a rapid outgassing to remove the air from the cell; the outgassing time was kept as short as possible, in order to avoid any possible Pd^{2+} auto-reduction. In order to minimize changes on the catalyst surface, due to the reaction of the CO probe with the supported Pd-hydroxide phase, FT-IR experiments were performed by dosing CO (equilibrium pressure P_{CO} = 5 Torr) on samples pre-cooled down to 100 K. For comparison, the same experiment was performed also on samples heated at 393 K in vacuum and on 5PdAl reduced in H_2 gas at 393 K. A second set of experiments was aimed to characterize the surface sites on the reduced Pd particles by FT-

IR of CO adsorbed at room temperature, following the approach already discussed in our previous works [14,15,17,31]. In that case, the Pd phase was pre-reduced in H_2 gas at 373 K. The reduction process consisted in two subsequent H_2 dosages (equilibrium pressure P_{H2} = 120 Torr, contact time = 10 min), followed by outgassing at 373 K; then, the samples were cooled down to room temperature in a dynamic vacuum. All the outgassed samples were contacted *in situ* with CO (P_{CO} = 50 Torr); P_{CO} was then gradually decreased stepwise from 50 to 10^{-4} Torr, and the corresponding FT-IR spectra were recorded. The final spectrum corresponds to CO species irreversibly adsorbed at 300 K.

The intensities of all the FT-IR spectra reported in this work were normalized to the pellet weight in order to take into account the different optical thickness of the samples, *i.e.*, the quantity of Pd crossed by the IR beam. Consequently, as all samples contain the same amount of Pd, the reported intensity of a given IR absorption band along the whole set of samples is directly proportional to the amount of carbonyl species responsible of that band, so that all the spectra are directly comparable each other.

3. Results and discussion

3.1. Catalyst performances in the debenzylation of 4-benzyloxyphenol

The catalytic performances of unreduced and pre-reduced samples were tested in a debenzylation reaction, a widely used reaction in fine chemicals and pharmaceutical industry where functional groups protection or de-protection is required [32–34]. Herein, 4-benzyloxyphenol was selected as a model substrate. Upon hydrogenation, the C–O bond is cleaved, with the attendant production of toluene and hydroquinone, according to Scheme 1.

Table 1 summarizes the catalytic performances of all the investigated catalysts in terms of (i) induction time, (ii) activity and (iii) turnover frequency (TOF), calculated on the basis of the number of surface Pd atoms as obtained by CO chemisorptions measurements (vide infra). As far as unreduced catalysts are concerned, the activity linearly increases with Pd loading, being the TOF almost constant; the induction time decreases upon increasing the Pd concentration. Coming to the pre-reduced samples, all the recorded parameters are greatly affected by the pre-reduction treatment. The first and more evident effect is the disappearance of any induction time. Secondly, pre-reduced 5PdAl catalysts show a greater activity than the unreduced one and, consequently, a greater TOF.

The data summarized in Table 1 unequivocally indicate that the pre-reduction procedure affects the catalyst performance. However, its effects on the oxidation degree and reducibility of supported Pd phase, as well as the morphology, the structural order and the surface properties of final Pd nanoparticles were never investigated in detail. This would be of a great interest in view of a rational choice of the best preparation procedure. The following sections will deal with the investigation of each one of the above-mentioned catalyst properties. In most cases, the measurements were taken on 5PdAl and 5PdAl(F), the latter chosen as a representative for the pre-reduced catalysts.

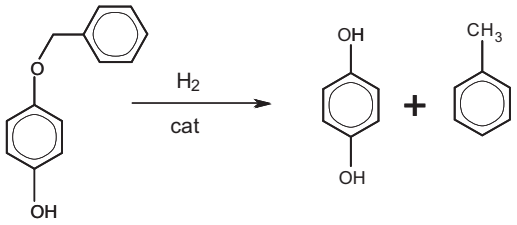

Scheme 1. Debenzylation of 4-benzyloxyphenol to form hydroquinone and toluene.

Table 1
Catalyst activity (in $cm^3\ min^{-1}$) and turnover frequency (TOF, s^{-1}, defined as the number of H_2 molecules consumed per second per number of surface atoms determined by CO chemisorption as an independent technique) of unreduced PdAl catalysts as a function of the Pd loading and of pre-reduced 5PdAl catalysts.

Sample	Induction time (min)	Activity ($cm^3\ min^{-1}$)	TOF (s^{-1})
2PdAl	27	5.0	0.098
3.5PdAl	20	6.2	0.071
5PdAl	11	11.3	0.093
5PdAl(F)	0	12.9	0.156
5PdAl(B)	0	13.7	0.176
5PdAl(H)	0	14.4	0.170

3.2. Oxidation state of the supported Pd phase

3.2.1. Oxidation degree: TPR results

The oxidation state of the supported Pd phase in both the unreduced and pre-reduced catalyst was evaluated at first by means of TPR, which is one of the most common techniques used to investigate the reducibility of supported metal species [35–37]. However, the experiments on palladium are complicated by the fact that reduction of Pd^{2+} precursors to Pd^0 starts below room temperature, thus requiring the use of an apparatus capable to operate also at a low temperature (in this work from 153 K). This is the reason why very few works in literature show TPR data on the reduction of supported Pd^{2+} compounds [8,15,38–40].

The TPR profiles of 5PdAl and 5PdAl(F) are shown in Fig. 2. The two curves are characterized by a reduction peak starting at temperature lower than 275 K due to the $Pd^{2+} \rightarrow Pd^0$ reduction, followed by a smaller negative peak centred around 330 K due to the decomposition of the Pd hydride formed at lower temperature. The integrated area below the positive peak (after correction for both bulk and surface hydride formation) gives the overall hydrogen consumption in the reduction process and allows to calculate the Pd^{2+} fraction present in each sample. The so obtained data are summarized in the last column of Table 2 and indicate that:

(1) In 5PdAl (sample **2** in Table 2), all the supported Pd is in the Pd^{2+} form within the accuracy of the technique (the Pd^{2+}/Pd_{tot} ratio is determined with an incertitude of ±0.03); therefore, no reduction to Pd^0 occurs during the impregnation step.

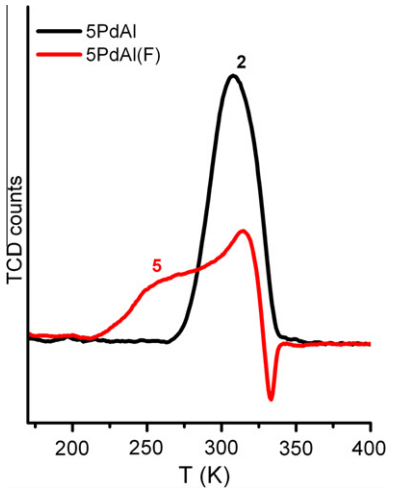

Fig. 2. TPR curves of 5PdAl (black) and 5PdAl(F) (red) samples dried in air at 393 K. The labels on the TPR curves refer to the sample code of Table 2. (For interpretation of the references to colour in this figure legend, the reader is referred to the web version of this article.)

Table 2
Summary of the TPR data obtained for 5PdAl and 5PdAl(F) samples subjected to different thermal treatments. Also, the data obtained for a bulk, unsupported, PdO sample are reported for comparison (samples **0** and **1**). T_{start} and T_{max} refer, respectively, to the starting and maximum temperature values of the hydrogen consumption peak due to the $Pd^{2+} \rightarrow Pd^0$ reduction; Pd^{2+}/Pd_{tot} is the fraction of Pd^{2+} present in the catalyst (see Section 3.2).

Code	Sample	Treatment	T_{start} (K)	T_{max} (K)	Pd^{2+}/Pd_{tot}
0	PdO	Air 393 K	260	298	1.00
1	PdO	H_2 393 K + air 393 K	173	198	0.16
2	5PdAl	Air 393 K	265	308	0.97
2′	5PdAl	N_2 393 K	247	271	1.02
3	5PdAl	H_2 393 K	–	–	0.00
4	5PdAl	H_2 393 K + air 300 K	175	256	0.35
5	5PdAl(F)	Air 393 K	213	315	0.57
5′	5PdAl(F)	N_2 393 K	163	223	0.58
6	5PdAl(F)	H_2 393 K	–	–	0.00
7	5PdAl(F)	H_2 393 K + air 300 K	172	n.d.	0.25
8	5PdAl(F)	H_2 393 K + air 393 K	201	301	0.52

(2) In 5PdAl(F) (sample **5** in Table 2), more than half of the Pd phase is still oxidized. The TPR results are confirmed by XANES and EXAFS data (not shown). This observation is quite unexpected since the catalyst was reduced in Na-formate. It is worth underlining that the fraction of Pd^{2+} (0.57–0.58) is much larger than that expected for a surface passivation, *i.e.*, formation of a surface monolayer of oxygen [26]; in such a case, the Pd^{2+} fraction value would be of 0.24, as calculated on account of the dispersion values obtained from CO chemisorption data (vide infra). The same extent of subsurface oxidation is observed also when PdAl(F) is dried in inert atmosphere (sample **5′** in Table 2), demonstrating that Pd is partially oxidized already in the wet sample and that drying in air did not alter the Pd^{2+} fraction.
(3) Although it is still highly oxidized, 5PdAl(F) starts to be reduced at lower temperature than PdAl.

In principle, the presence of about 50% of oxidized Pd in the 5PdAl(F) sample (see Table 2) can be explained by two main hypothesis: (i) incomplete reduction of the supported Pd-hydroxide by Na-formate; (ii) re-oxidation of fully reduced Pd^0, due to later exposure of the wet catalyst to air. The Pd surface would be oxidized in any case, since it is well known that O_2 chemisorbs dissociatively on metal Pd [41–43]. However, in the case (i), both the core and the surface of the Pd particles should be oxidized, whereas in the case (ii), the oxidation process should involve only the surface and the subsurface layers. In order to get more insight into the nature of the partially oxidized Pd particles in the PdAl(F) sample, a sequence of TPR measurements was taken on a PdAl sample subjected to *ad hoc* conceived thermal treatments. The TPR curves are shown in Fig. 3, whereas the corresponding T_{start} and T_{max} values, as well as the Pd^{2+} fraction are summarized in Table 2.

The TPR profile of 5PdAl(F) reduced in H_2 gas (sample **6** in Fig. 3 and Table 2) showed no consumption of H_2 but only the hydride decomposition peak at 328 K demonstrating that thermal treatment in H_2 gas causes a complete $Pd^{2+} \rightarrow Pd^0$ reduction (in agreement with XAS results, not shown). When the sample is exposed to air at room temperature (sample **7** in Fig. 3 and Table 2), Pd^0 is partially re-oxidized, as testified by the appearance of the $Pd^{2+} \rightarrow Pd^0$ reduction peak. However, the re-oxidized Pd is only a fraction of the total Pd (about 25%) and likely corresponds to a surface monolayer only (dispersion = 24%, vide infra). A larger fraction of Pd^0 (52%) is re-oxidized when the 5PdAl(F) sample reduced in H_2 gas is treated in air at 393 K (sample **8** in Fig. 3 and Table 2). In addition, the thinner the re-oxidized Pd^{2+} layer, the easier its reduction (*i.e.*, lower T_{start} and T_{max}), probably as a result of surface defectivity. The shape as well as T_{start}, T_{max}, and the integrated area of the TPR reduction peak of sample 5PdAl(F) dried in air (sample **5** in Fig. 3 and Table 2) are close to that of sample 5PdAl(F) reduced in H_2 gas and treated in air at 393 K (sample **8** in Fig. 3 and Table 2). Because the latter is covered by an external PdO layer formed during re-oxidation of the fully reduced Pd, the result supports the hypothesis (ii) formulated above: Na-formate fully reduces the supported Pd-hydroxide phase; then, the resulting Pd^0 is partially re-oxidized by air on both, surface and subsurface.

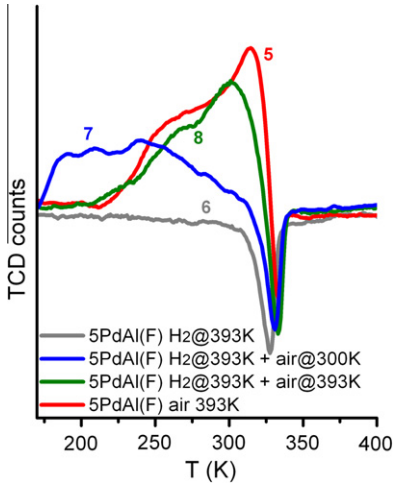

Fig. 3. TPR signals for 5PdAl(F) reduced in H_2 at 393 K (grey) and of the same sample successively treated in air at 300 K (blue) and 393 K (green), compared to the TPR signal of 5PdAl(F) dried in air at 393 K (red). The labels on the TPR curves refer to the sample code of Table 2. (For interpretation of the references to colour in this figure legend, the reader is referred to the web version of this article.)

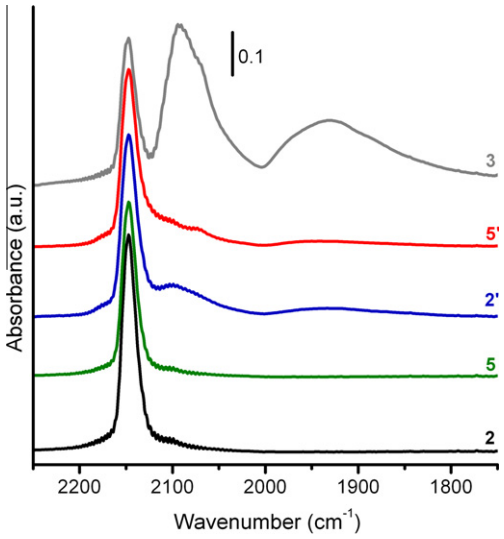

Fig. 4. FT-IR spectra of CO adsorbed at 100 K on 5PdAl and 5PdAl(F) samples dried either in air (black and green spectra) or in vacuum (blue and red spectra) at 393 K, compared to the spectrum obtained in the same conditions on 5PdAl reduced in H_2 at 393 K (grey). The numeric labels refer to the sample code of Table 2. (For interpretation of the references to colour in this figure legend, the reader is referred to the web version of this article.)

3.2.2. Surface oxidation state: FT-IR of CO adsorbed at 100 K

In order to definitely demonstrate that the Pd phase in 5PdAl(F) has a metal core-oxide layer structure, we have performed a FT-IR experiment of CO adsorbed at 100 K. The low temperature is necessary to avoid reaction of CO with the supported Pd^{2+} phase

[20,44–46]. Fig. 4 shows the FT-IR spectra of CO adsorbed at low temperature on the 5PdAl and 5PdAl(F) samples dried in air at 393 K (samples **2** and **5**, respectively). Both spectra are dominated by an IR absorption band at around 2148 cm^{-1}, which is due to CO physisorbed on the support [47], whereas no IR absorption bands at frequencies lower than 2100 cm^{-1} are observed for both samples, demonstrating that no accessible metal Pd is present in those cases. Apparently, no IR absorption bands ascribable to carbonyl species formed on Pd^{2+} species are observed. However, linear carbonyls on Pd^{2+} sites have been reported to give absorption in the 2160–2140 cm^{-1} range [20,44–46,48–51], that is precisely the frequency range dominated by the IR absorption band due to physisorbed CO.

The same experiment was repeated for 5PdAl and 5PdAl(F) dried in vacuum, with the aim to exclude that the absence of accessible Pd^0 sites on 5PdAl(F) was induced by the drying procedure in air. The corresponding FT-IR spectra (samples **2′** and **5′**, respectively) show, in addition to the IR absorption band due to physisorbed CO, very weak IR absorption bands around 2100 and 1950 cm^{-1} characteristic of carbonyls formed on Pd^0 [14,17,20,31,52–61]. However, these bands are much less intense than those obtained by dosing CO on 5PdAl sample reduced in H_2 at 393 K (sample **3**, grey spectrum in Fig. 4) and are assigned to CO adsorbed on the small fraction of defective sites that have been auto-reduced during the sample activation (see Section 2). The FT-IR spectra shown in Fig. 4 validate the hypothesis formulated above on the basis of TPR results: the surface oxidation state of the supported Pd phase is +2 for both, 5PdAl and 5PdAl(F) samples.

3.3. Reducibility of oxidized samples

In the previous paragraphs, we have demonstrated that the surface of Pd particles is fully oxidized in both unreduced and pre-reduced catalysts. Thus, the oxidation state of Pd surface sites cannot be accounted for the different catalytic performances induced by pre-reduction. An alternative explanation comes from the observation that 5PdAl(F) is reduced at temperature lower than 5PdAl, as already shown in Fig. 2 and summarized in Table 2. This result suggests that the two oxidized phases in 5PdAl and 5PdAl(F) have different properties.

The easier reducibility of 5PdAl(F) can be explained by analyzing the results of TPR experiments summarized in Fig. 5, where the starting reduction temperature T_{start}, which is the most significant parameter indicating the easiness of catalyst reduction, is reported versus the Pd^{2+} fraction in the samples. The data shown in Fig. 5 are a selection of those reported in Table 2 and include samples at different degrees of oxidation: (i) the two fully oxidized samples 5PdAl (sample **2**) and bulk PdO (sample **0**), (ii) the partially oxidized sample 5PdAl(F) (sample **5**), and (iii) the partially oxidized samples obtained from 5PdAl, 5PdAl(F), and PdO reduced at 393 K in H_2 and re-oxidized in air at RT and 393 K. All the data lie on a straight line, meaning that more oxidized are the Pd particles, less easy is their reduction. It is well known that re-oxidation of metal Pd causes an increase in surface irregularity, up to a surface fragmentation [62–64]. This is a consequence of both the larger volume of PdO with respect to that of metal Pd and its lower surface tension. However, by increasing the oxidation degree, the oxidized layer becomes progressively more regular approaching the order of true oxide, such as in samples 5PdAl and bulk PdO. The easier reducibility of 5PdAl(F) with respect to 5PdAl would be the consequence of a greater disorder of the few external PdO layers when compared to the bulk-like PdO phase in 5PdAl.

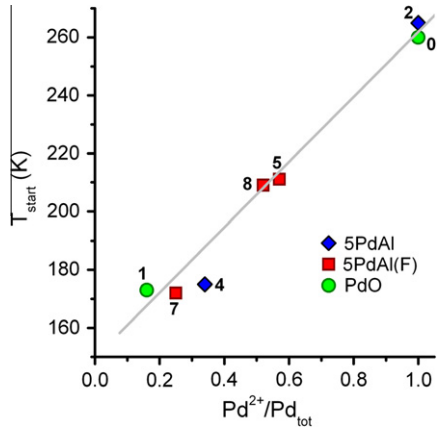

Fig. 5. Starting reduction temperature (T_{start}) as a function of the Pd^{2+} fraction in the catalysts as determined by TPR experiments. The labels on the scattered points refer to the sample code of Table 2.

3.4. Properties of reduced Pd

The data shown in the previous sections definitely demonstrate that, in spite of a large amount of oxidized Pd phase still present, the pre-reduced 5PdAl(F) catalyst is reduced more easily than the unreduced one. However, once the catalysts are in the reducing reaction environment, it could be that the starting differences vanish. Therefore, it is important to know whether the different reducibility observed on the fresh catalysts corresponds to different properties, such as particle size, morphology, and defectivity, of the Pd nanoparticles in the reducing environment (i.e., during the catalytic act), thus explaining the different observed catalytic performances (see Table 1). A direct investigation on both 5PdAl and 5PdAl(F) samples after reduction in reaction conditions would be complicated by several factors, including the possible presence of compounds from reaction medium; therefore, the samples have been treated in H_2 gas at 393 K in order to completely reduce the Pd phase.

3.4.1. Pd dispersion and interaction of Pd particles with the support (CO chemisorption, TEM, and SAXS)

CO chemisorption was already demonstrated to be an efficient technique for investigating the dispersion of Pd nanoparticles (i.e., the ratio between surface and total metal atoms) when poisoning phenomena of the exposed metal surface are negligible [8,14]. From the dispersion values summarized in Table 3, it is evident that Pd dispersion (D_{chemi}) slightly decreases with increasing Pd concentration, as already reported in literature. Moreover, the pre-reduced catalysts show a lower dispersion than the unreduced one, independently of the reducing agent.

A first hypothesis to explain the loss of Pd dispersion after pre-reduction in liquid phase is the occurrence of a relevant sintering of the Pd particles; in this case, TEM investigation should reveal an increase in the average particle diameter going from unreduced

Table 3
Pd dispersion as obtained by CO chemisorption data (D_{chemi}) and, when available, by SAXS data (D_{SAXS}), minimum of the negative peak due to the decomposition of the formed Pd hydride (T_{min}) and corresponding H/Pd in Pd hydride, as obtained by TPR on the whole set of samples investigated in this work.

Sample	D_{chemi} (%)	D_{SAXS} (%)	T_{min} (K)	H/Pd in Pd hydride
PdO	0.2	–	339	0.50
2PdAl	38	n.a.	321	0.17
3.5PdAl	37	n.a.	320	0.17
5PdAl	36	38	322	0.19
5PdAl(F)	24	31	328	0.27
5PdAl(B)	23	31	329	0.29
5PdAl(H)	25	32	327	0.28

to pre-reduced catalysts. For this reason, a series of TEM images were collected on both 5PdAl and 5PdAl(F); three representative images are shown in Fig. 6a–c. In all cases, Pd particles having a fcc structure (as evidenced by electron diffraction, see insets in Fig. 6a–c) are homogeneously distributed on the support in an isolated form, whereas no aggregates are observed (Figure not shown). A careful analysis of several TEM images revealed that the average Pd particle size increases moderately after the reduction process, but it cannot account for the whole loss of Pd dispersion as found by CO chemisorption. Unfortunately, it is not possible to quantitatively estimate the change in particle size as already done in previous cases [14,15], mainly because the cubo-octahedral morphology of Pd particles exhibits (1 1 1) and (1 0 0) faces in different ratio (see arrows and labels in Fig. 6) that makes difficult the identification of the particle diameter. As an example, Fig. 6b shows a Pd particle terminating mainly with (1 1 1) faces, whereas in the Pd particle shown in Fig. 6a and c, the extension of (1 0 0) faces is larger. In all the cases, the particle diameter would result in a different value according to the direction in which it is evaluated. As TEM provides only the projection of the particle on the plane perpendicular to the electron beam axis, and not a tri-dimensional reconstruction of the particles, a reliable particle size distribution cannot be obtained in the present conditions, contrarily to what done in the past on samples characterized by particles with symmetrical shape [14,15].

On the contrary, quantitative information on the particle size distribution was obtained by SAXS measurements. With respect to TEM, SAXS technique has the advantage to get information on the whole particles population. Fig. 7a shows, as an example, the experimental SAXS curve for 5PdAl (red circles) compared to that of the bare γ-Al_2O_3 support (grey full line). The experimental SAXS profiles of the pre-reduced sample (not reported) have a similar signal-to-noise ratio. Overlapped to the experimental data in Fig. 7a, also the best fit (black full line) and the theoretical signal obtained by considering a distribution of spherical Pd particles (dotted line) are reported. The fit has been performed optimizing a scale factor for the support contribution (accounting for a slightly different packing of the two capillaries) and the Pd particle size distribution in terms of a mean value and a σ for a log-normal distribution [65,66]. Fig. 7b displays the particle size distribution obtained by analyzing the SAXS data of 5PdAl and of the pre-reduced samples. For 5PdAl, the Pd particle size is centred around 1.5 nm, corresponding to a dispersion D_{SAXS} = 38% (Table 3) [14]. The particle size distribution for the three pre-reduced catalysts is centred around the same average value as 5PdAl, but presents a tail toward greater values, resulting into slightly lower D_{SAXS} values with respect to 5PdAl (Table 3). These results provide a clear and quantitative evidence that the pre-reduction causes an increase in the Pd particle size. However, the decrease in D_{SAXS} by going from unreduced to pre-reduced samples is smaller than the decrease in D_{chemi}. This means that the increase in the Pd particles size cannot account for all the loss of dispersion measured by CO chemisorption data, suggesting that in the pre-reduced samples, not all the surface of the Pd particles is accessible to the CO probe.

As a matter of fact, in addition to the moderate increase in Pd particle size by going from 5PdAl to 5PdAl(F), TEM images revealed the occurrence of an embedding of the Pd particles into the Al_2O_3 support, a phenomenon that undoubtedly contributes to the loss of Pd dispersion after reduction in the liquid phase. In fact, although already a fraction of Pd particles were partially buried into Al_2O_3 in 5PdAl sample, an important fraction was protruding out of the surface (an example is shown in Fig. 6c). In contrast, nearly all the Pd particles are partially embedded into the support in 5PdAl(F) sample (Fig. 6b). A strong metal–support interaction is typically observed in the presence of highly reducible supports (such as TiO_2 and CeO_2), and in those cases, H_2 reduction at high temperature ($\geqslant$773 K) brings about a relevant decrease in the chemisorption ability of the metal. Although the final effect is similar, the phenomenon discussed herein has a different origin and reflects a high mobility of the Al_2O_3 support, even in the absence of H_2 at high temperature. Recently, we have shown that relevant

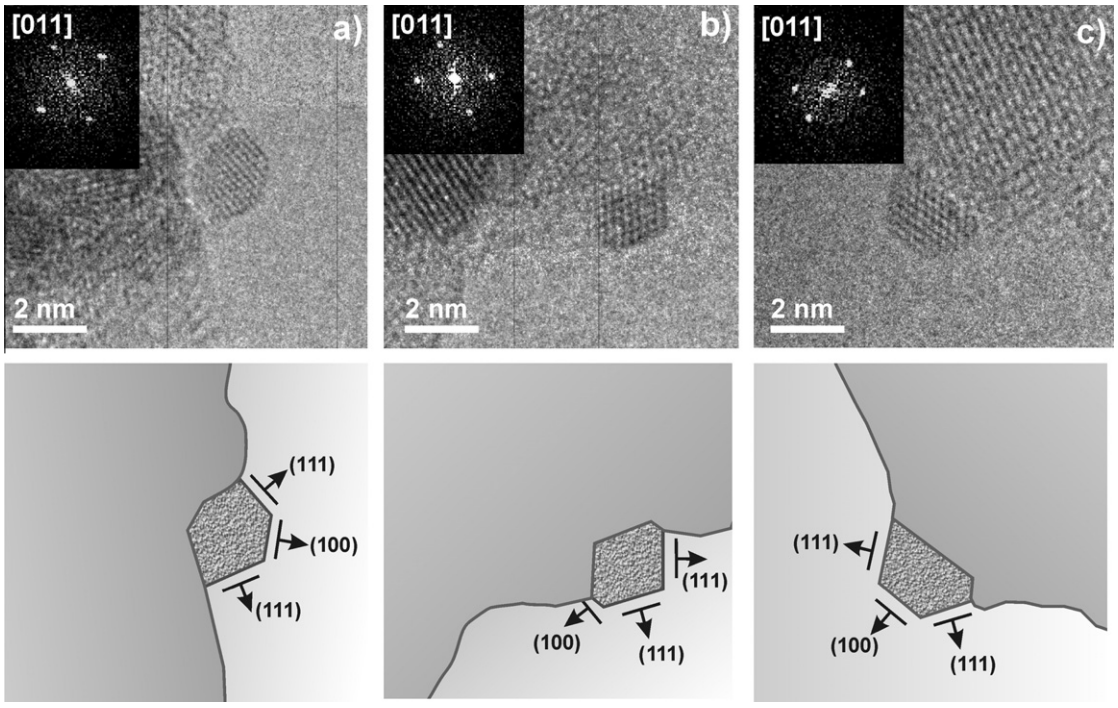

Fig. 6. Selected TEM micrographs of a few Pd particles on both 5PdAl (parts a and c) and 5PdAl(F) (part b) samples (top part) and schematic representation of the exposed faces (bottom part). The insets show the electron diffraction of each particle, demonstrating the fcc structure.

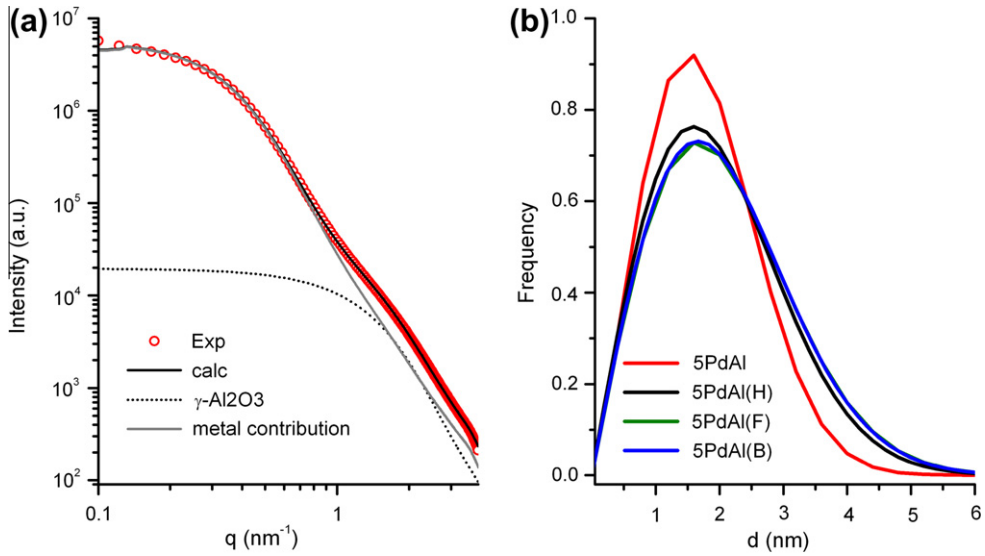

Fig. 7. Part (a): Experimental SAXS curve of 5PdAl (dots) compared to the signal of the bare Al support (grey). Also, the theoretical signal obtained by considering spherical Pd particles (dotted line) and the best fit (black line) is reported. Part (b): particle size distribution for the unreduced and pre-reduced samples obtained by analyzing the SAXS data.

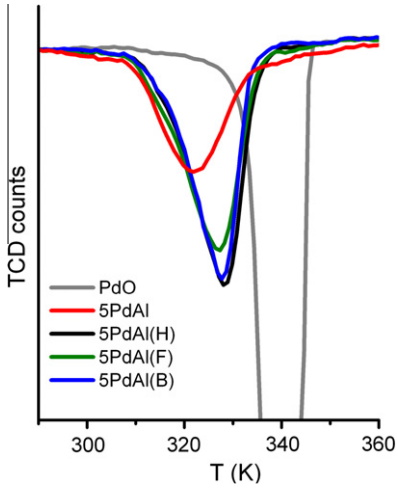

Fig. 8. TPR signals of PdO bulk, unreduced, and pre-reduced catalysts dried in air at 393 K and then reduced in H_2 at 393 K, in the region of the negative peak due to hydride decomposition.

changes in the morphology of some supports (*e.g.*, γ-Al_2O_3 and SiO_2–Al_2O_3) can occur during catalyst preparation [16]. In particular, an increase in surface area and decrease in the pore volume were observed on γ-Al_2O_3 after the Pd precipitation. These morphological changes were attributed to the mobility of Al_2O_3, induced by the basic medium used during Pd deposition–precipitation. The presence of a fraction of Pd particles embedded in the support already in 5PdAl (see Fig. 6a) is in agreement with the results discussed above. The phenomenon becomes much more evident in 5PdAl(F) because the catalyst remains for longer time in an alkaline solution (Na-formate used for reduction), thus favouring a further mobility of the Al_2O_3 support. Summarizing, reduction in the liquid phase brings about a decrease in Pd dispersion that is partially explained by a sintering of Pd particles (quantitatively determined by SAXS measurements) and partially by their embedding into Al_2O_3 (which is observed by TEM and explains the discrepancy between D_{chemi} and D_{SAXS} for the pre-reduced catalysts), due to the high mobility of the support in the alkaline environment characterizing the catalyst preparation.

3.4.2. Pd disorder (TPR and FT-IR of adsorbed CO)

Additional information on the properties of the supported Pd particles can be obtained by TPR data in the region of the negative peak due to hydride decomposition. A magnification of TPR curves of 5PdAl and pre-reduced samples in the Pd hydride decomposition region is shown in Fig. 8. All the samples were subjected to the same treatment performed during CO chemisorption measurements, *i.e.*, drying in air at 393 K followed by reduction in H_2 at the same temperature. The curves of unreduced and pre-reduced samples differ in both integrated area of the negative peak and peak position. The integrated area allows the calculation of the H/Pd ratio in Pd hydride, as summarized in Table 3. The temperature of hydride decomposition appears to be strictly correlated to H/Pd ratio suggesting that both of them are dependent on the same property. As already pointed out, the reduction in liquid medium confers to Pd particles specific characteristics, independently on reductant.

It is well known that the H/Pd value decreases upon increasing the Pd dispersion; the same trend is shown by the temperature of the hydride decomposition [39,67–74]. However, both quantities depend also on the internal disorder of the Pd particles, due to both framework defects, impurities or decorations: the lower the H/Pd ratio, the more disordered the Pd particles [68–70,72,74–76]. The two factors affecting the H/Pd ratio and the decomposition temperature of the hydride are often correlated each other because the smallest particles tend to be more disordered than the bigger ones [75]. Thus, it is difficult to decide the importance of the relative contribution of the two characteristics, *i.e.*, particle size and internal disorder, to H/Pd ratio and decomposition temperature. According to TEM and SAXS evaluations, that point out only a modest difference of Pd particle size between 5PdAl and 5PdAl(F), we must conclude that the Pd particles of the unreduced catalyst are more disordered than those of pre-reduced ones, probably because of the milder conditions and slower rate of the reduction in liquid medium with respect to those of reduction with H_2 in gas phase.

FT-IR spectroscopy of adsorbed CO has been used to obtain information on the surface regularity of the final Pd particles; these data provide information complementary to those obtained by TPR, which gave indication on the Pd disorder in the bulk. Indeed, FT-IR spectroscopy of adsorbed CO is a well-established technique to obtain information on the exposed faces of supported metal

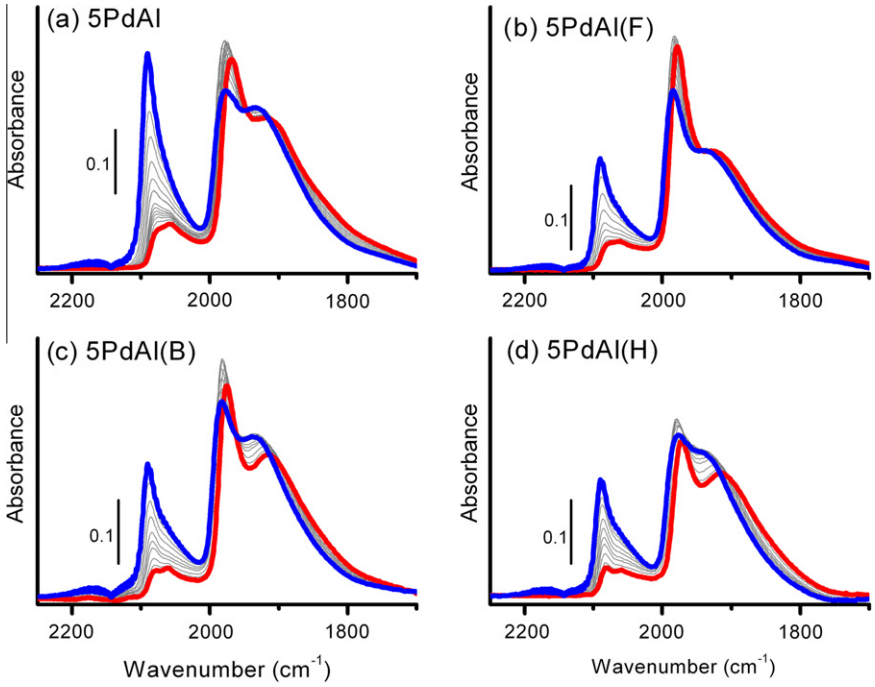

Fig. 9. FT-IR spectra of CO adsorbed at room temperature on unreduced and pre-reduced samples, reduced in H_2 at the 393 K. The sequences of FT-IR spectra show the effect of decreasing P_{CO}, from 50 Torr (blue spectrum) to 10^{-4} Torr (red). (For interpretation of the references to color in this figure legend, the reader is referred to the web version of this article.)

nanoparticles and on their defectivity [14,17,20,31,52–61]. The FT-IR spectra of CO adsorbed at room temperature on unreduced and pre-reduced samples subjected to the same treatment performed during CO chemisorption measurements (*i.e.*, dried in air at 393 K and successively reduced in H_2 at the same temperature) are shown in Fig. 9 as a function of CO pressure. In our experimental conditions, θ_{max} (blue curve) corresponds to $T = 300$ K and $P_{CO} = 50$ Torr, whereas θ_{min} (red curve) is obtained by evacuation at 300 K down to 10^{-4} Torr. In all cases, the IR spectrum at the maximum CO coverage (blue) shows three main IR absorption bands at around 2090, 1940, and 1985 cm^{-1}, which are the characteristic of linear and bridged carbonyls on (111) faces and of bridged carbonyls on (100) faces, respectively [17,20,55,58,77–91]. Therefore, FT-IR spectra are in good agreement with the morphology determined by TEM images (Fig. 6), which showed Pd particles terminating with (111) and (100) faces in different proportion. All of the above-mentioned IR absorption bands evolve upon decreasing CO pressure, as a consequence of the decreasing CO population, as it is well known in literature [17,20,55,58,77–91]. In particular, linear carbonyls are the most reversible adsorbed species and the corresponding IR absorption band downward shifts of about 15 cm^{-1}, because of the removal of coupling between adjacent CO oscillators. At lower CO coverage, an additional IR absorption band around 2050 cm^{-1} emerges, which is assigned to linear carbonyls on defective sites; these species are irreversible upon outgassing at room temperature.

Two main differences are observed between the FT-IR spectra of CO adsorbed on 5PdAl and those of CO adsorbed on the pre-reduced samples. Although the types of surface Pd carbonyls are the same (same frequency position of all the IR absorption bands), their relative amount is different (different relative intensity of the three IR absorption bands). In particular, by comparing the IR spectra at the highest CO coverage, the following differences can be noticed: (i) the IR absorption bands characteristic of linear and bridged carbonyls have an almost equal intensity in 5PdAl, whereas for the three pre-reduced samples, the IR absorption band due to linear carbonyls has a lower intensity; (ii) the IR absorption band at 1985 cm^{-1}, assigned to bridged carbonyls on (100) faces, is scarcely visible in 5PdAl, suggesting that (100) faces are less extended than (111) faces. The same IR absorption band is more prominent in the IR spectra of CO adsorbed on the three pre-reduced samples. A correlation between the Pd particle size and the relative proportion of linear and bridged carbonyls in the IR spectra of adsorbed CO has been already established [92,93]. On small and amorphous (*i.e.*, highly defective) metal particles, CO is adsorbed prevalently in the linear (terminal) mode, whereas an increase in the particle size (and thus in the order) results in the formation of a greater number of bridged carbonyls [17,55,60,92–95]. On these bases, the overall sequence of FT-IR spectra shown in Fig. 9 points out that Pd particles on 5PdAl display a more defective surface than those on the pre-reduced catalysts. Therefore, pre-reduction in liquid phase would be responsible for the formation of bigger Pd particles more ordered, both internally (as obtained by TPR) and on the surface (as shown by FT-IR spectroscopy of adsorbed CO).

4. Conclusions

The present work investigates the relationship between the reduction state of Pd-based alumina-supported catalysts as loaded into the reactor, and their properties and catalytic performances in the debenzylation of 4-benzyloxyphenol. It was found that, after pre-reduction in the liquid phase, about 50% of the Pd in the catalyst is still oxidized. The reason is attributed to a partial re-oxidization of the Pd^0 particles formed during the reduction step, because of the contact of wet catalyst with the air. The re-oxidation involves both, surface and subsurface. However, the external Pd^{2+} phase is easier to be reduced than bulk PdO; therefore, the pre-reduced catalyst starts faster in reaction conditions, as testified by the absence of an induction time in the adopted experimental conditions. The easier reducibility of the pre-reduced catalyst has been

explained as due to the greater structural disorder of a few external PdO layers when compared to a bulk PdO.

Besides affecting the catalyst reducibility, the pre-reduction in liquid phase influences also the properties of the final Pd nanoparticles in many aspects and, consequently, the catalyst performances. In particular, the Pd dispersion decreases (CO chemisorption data, Table 3) mainly as a consequence of: (i) a greater interaction of the Pd particles with the support (embedding), as observed by TEM (Fig. 6), and (ii) a particle sintering (as suggested qualitatively by TEM and demonstrated quantitatively by SAXS). Moreover, the pre-reduction in liquid phase brings to an increase in the order (both internal and superficial) of the Pd particles (TPR and FT-IR data, Fig. 8 and Fig. 9). As a consequence, the final Pd particles display (qualitatively) the same types of active sites in the two catalysts, although in different proportion. In particular, Pd particles in pre-reduced catalysts are bigger than those in unreduced one and more ordered both internally and on the surface; as a consequence, the latter have a larger fraction of sites located on extended faces, than on edges or corners. A greater structural order of supported Pd particles would favour the debenzylation of 4-benzyloxyphenol as well as other surface-sensitive reactions.

Acknowledgments

Luca Diano is kindly acknowledged for performing some of the FT-IR experiments. We are indebted with the whole staff of DUBBLE BM26 beamline at the ESRF (particularly to Daniel Hermida Merino, S. Nikitenko, and W. Brass) where both Pd K-edge EXAFS (BM26A) and SAXS (BM26B) measurements were taken. We are particularly grateful to Andrea Governini (Chimet SpA) for the catalytic activity measurements and to Massimo Graziani (Chimet SpA) for the chemisorption measurements. The authors wish to thank Adriano Zecchina and Francesco Giannici for the stimulating discussion.

References

[1] H.-U. Blaser, A. Indolese, A. Schnyder, H. Steiner, M. Studer, J. Mol. Catal. A: Chem. 173 (2001) 3.
[2] N. Pernicone, M. Cerboni, G. Prelazzi, F. Pinna, G. Fagherazzi, Catal. Today 44 (1998) 129.
[3] D. Duca, F. Arena, A. Parmaliana, G. Deganello, Appl. Catal., A 172 (1998) 207.
[4] F. Figueras, B. Coq, J. Mol. Catal. A: Chem. 173 (2001) 223.
[5] E. Santacesaria, P. Wilkinson, P. Babini, S. Carra, Ind. Eng. Chem. Res. 27 (1988) 780.
[6] G. Neri, M.G. Musolino, C. Milone, D. Pietropaolo, S. Galvagno, Appl. Catal. A: Gen. 208 (2001) 307.
[7] M. Studer, H.U. Blaser, J. Mol. Catal. A: Chem. 112 (1996) 437.
[8] G. Agostini, E. Groppo, A. Piovano, R. Pellegrini, G. Leofanti, C. Lamberti, Langmuir 26 (2010) 11204.
[9] K.G. Griffin, S. Hawker, M.A. Batti, The removal of protecting groups by catalytic hydrogenation, in: R.E. Malz (Ed.), Catalysis of Organic Reactions, Marcel Dekker, Inc., 1996.
[10] W.M. Pearlman, Tetrahedron Lett. 8 (1967) 1663.
[11] A.M.R. Galletti, F. Bonaccorsi, F. Calvani, C. Di Bugno, Catal. Commun. 7 (2006) 896.
[12] H.-U. Blaser, U. Siegrist, H. Steiner, Aromatic nitro compounds, in: R.A. Sheldon, H. van Bekkum (Eds.), Fine Chemicals through Heterogeneous Catalysis, Wiley-VCH, Weinheim, 2001.
[13] E. Auer, A. Freund, J. Pietsch, T. Tacke, Appl. Catal. A: Gen. 173 (1998) 259.
[14] G. Agostini, R. Pellegrini, G. Leofanti, L. Bertinetti, S. Bertarione, E. Groppo, A. Zecchina, C. Lamberti, J. Phys. Chem. C 113 (2009) 10485.
[15] R. Pellegrini, G. Leofanti, G. Agostini, L. Bertinetti, S. Bertarione, E. Groppo, A. Zecchina, C. Lamberti, J. Catal. 267 (2009) 40.
[16] R. Pellegrini, G. Leofanti, G. Agostini, M. Rivallain, E. Groppo, C. Lamberti, Langmuir 25 (2009) 6476.
[17] E. Groppo, W. Liu, O. Zavorotynska, G. Agostini, G. Spoto, S. Bordiga, C. Lamberti, A. Zecchina, Chem. Mater. 22 (2010) 2297.
[18] P. Kasai, R. Bishop, J. Phys. Chem. 81 (1977) 152.
[19] J. Michalik, M. Narayama, L. Kevan, J. Phys. Chem. 89 (1985) 4553.
[20] D. Tessier, A. Rakai, F. Bozonverduraz, J. Chem. Soc. Faraday Trans. 88 (1992) 741.
[21] M. Boudart, Chem. Rev. 95 (1995) 661.
[22] W.R. Alcorn, T.J. Sullivan, Evaluation of hydrogenation catalysts in batch reactors, in: J.R. Kosak (Ed.), Catalysis of Organic Reactions, Marcel Dekker, Inc., 1984.
[23] H.S. Fogler, Elements of Chemical Reaction Engineering, Prentice-Hall Inc., 1992.
[24] G.W. Roberts, The influence of mass and heat transfer on the performance of the heterogeneous catalysts in gas/liquid/solid systems, in: P.N. Rylander, H. Greenfield (Eds.), Catalysis in Organic Synthesis, Academic Press, 1976.
[25] J.R. Anderson, K.C. Pratt, Surface Area Measurement, In Introduction to Characterization and Testing of Catalysts, Academic Press, 1986.
[26] G. Prelazzi, M. Cerboni, G. Leofanti, J. Catal. 181 (1999) 73.
[27] W. Bras, I.P. Dolbnya, D. Detollenaere, R. van Tol, M. Malfois, G.N. Greaves, A.J. Ryan, E. Heeley, J. Appl. Crystall. 36 (2003) 791.
[28] A.P. Hammersley, ESRF Internal Report, ESRF98HA01T, FIT2D V9.129 Reference Manual V3.1, 1998.
[29] A. Longo, P. Calandra, M.P. Casaletto, C. Giordano, A.M. Venezia, V. Turco Liveri, Mater. Chem. Phys. 96 (2006) 66–72.
[30] E. Cattaruzza, F. D'Acapito, F. Gonella, A. Longo, A. Martorana, G. Mattei, C. Maurizio, D. Thiaudière, Appl. Cryst. 33 (2000) 740.
[31] E. Groppo, S. Bertarione, F. Rotunno, G. Agostini, D. Scarano, R. Pellegrini, G. Leofanti, A. Zecchina, C. Lamberti, J. Phys. Chem. C 111 (2007) 7021.
[32] M. Freifelder, Practical Catalytic Hydrogenation Techniques and Applications, John Wiley & Sons, Inc., 1971.
[33] S. Nishimura, Handbook of Heterogeneous Catalytic Hydrogenation for Organic Synthesis, John Wiley & Sons, Inc., 2001.
[34] L.S. Seif, K.M. Partyka, J.E. Hengeveld, Selective hydrogenolysis of benzyl and carbobenzyloxy protecting groups for hydroxyl and amino functions, in: D.W. Blackburn (Ed.), Catalysis of Organic Reactions, Marcel Dekker, Inc., New York, 1990.
[35] H. Knözinger, Temperature-programmed reduction and oxidation, in: Handbook of Heterogeneous Catalysis, 2008.
[36] N.W. Hurst, S.J. Gentry, A. Jones, B.D. McNicol, Catal. Rev. 24 (1982) 233.
[37] J.W. Niemantsverdriet, Temperature-programmed techniques, in: Spectroscopy in Catalysis: An Introduction, Wiley-VCH, 2007.
[38] B.C. Campo, M.A. Volpe, C.E. Gigola, Ind. Eng. Chem. Res. 48 (2009) 10234.
[39] C. Amorim, M.A. Keane, J. Colloid Interface Sci. 322 (2008) 196.
[40] C.W. Chou, S.J. Chu, H.J. Chiang, C.Y. Huang, C.J. Lee, S.R. Sheen, T.P. Perng, C.T. Yeh, J. Phys. Chem. B 105 (2001) 9113.
[41] H. Conrad, G. Ertl, J. Kiippers, E.E. Latta, Surf. Sci. 65 (1977) 245.
[42] T.W. Orent, S.D. Bader, Surf. Sci. 115 (1982) 323.
[43] M. Peuckert, J. Phys. Chem. 89 (1985) 2481.
[44] G. Perez-Osorio, F. Castillon, A. Simakov, H. Tiznado, F. Zaera, S. Fuentes, Appl. Catal. B: Environ. 69 (2007) 219.
[45] H.Q. Zhu, Z.F. Qin, W.J. Shan, W.J. Shen, J.G. Wang, J. Catal. 233 (2005) 41.
[46] H. Tiznado, S. Fuentes, F. Zaera, Langmuir 20 (2004) 10490.
[47] C. Morterra, G. Magnacca, Catal. Today 27 (1996) 497.
[48] A. Palazov, C.C. Chang, R.J. Kokes, J. Catal. 36 (1975) 338.
[49] W. Juszczyk, Z. Karpinski, I. Ratajczykowa, Z. Stanasiuk, J. Zielinki, L.L. Sheu, W.M.H. Sachtler, J. Catal. 120 (1989) 68.
[50] K. Moller, T. Bein, J. Phys. Chem. 94 (1990) 845.
[51] Z.C. Zhang, H.Y. Chen, W.M.H. Sachtler, J. Chem. Soc. Faraday Trans. 87 (1991) 1413.
[52] R. Craciun, W. Daniell, H. Knozinger, Appl. Catal. A: Gen. 230 (2002) 153.
[53] A.N. Pestryakov, V.V. Lunin, S. Fuentes, N. Bogdanchikova, A. Barrera, Chem. Phys. Lett. 367 (2003) 102.
[54] M. Skotak, Z. Karpinski, W. Juszczyk, J. Pielaszek, L. Kepinski, D.V. Kazachkin, V.I. Kovalchuk, J.L. d'Itri, J. Catal. 227 (2004) 11.
[55] S. Bertarione, D. Scarano, A. Zecchina, V. Johanek, J. Hoffmann, S. Schauermann, M.M. Frank, J. Libuda, G. Rupprechter, H.J. Freund, J. Phys. Chem. B 108 (2004) 3603.
[56] A.M.J. van der Eerden, T. Visser, A. Nijhuis, Y. Ikeda, M. Lepage, D.C. Koningsberger, B.M. Weckhuysen, J. Am. Chem. Soc. 127 (2005) 3272.
[57] T. Lear, R. Marshall, E.K. Gibson, T. Schutt, T.M. Klapotke, G. Rupprechter, H.J. Freund, J.M. Winfield, D. Lennon, Phys. Chem. Chem. Phys. 7 (2005) 565.
[58] T. Lear, R. Marshall, J.A. Lopez-Sanchez, S.D. Jackson, T.M. Klapotke, M. Baumer, G. Rupprechter, H.J. Freund, D. Lennon, J. Chem. Phys. 123 (2005). Art. No. 174706.
[59] T. Lear, R. Marshall, J.A. Lopez-Sanchez, S.D. Jackson, T.M. Klapotke, M. Baumer, G. Rupprechter, H.J. Freund, D. Lennon, J. Chem. Phys. 124 (2006) (Art. No. 069901).
[60] S. Bertarione, C. Prestipino, E. Groppo, D. Scarano, G. Spoto, A. Zecchina, R. Pellegrini, G. Leofanti, C. Lamberti, Phys. Chem. Chem. Phys. 8 (2006) 3676.
[61] L. Bollmann, J.L. Ratts, A.M. Joshi, W.D. Williams, J. Pazmino, Y.V. Joshi, J.T. Miller, A.J. Kropf, W.N. Delgass, F.H. Ribeiro, J. Catal. 257 (2008) 43.
[62] J.J. Chen, E. Ruckenstein, J. Phys. Chem. 85 (1981) 1606.
[63] E.H. Voogt, A.J.M. Mens, O.L.J. Gijzeman, J.W. Geus, Surf. Sci. 350 (1996) 21.
[64] R.J. Farrauto, J.K. Lampert, M.C. Hobson, E.M. Waterman, Appl. Catal. B 6 (1995) 263.
[65] J.S. Pedersen, J. Appl. Crystallogr. 27 (1994) 595.
[66] J.S. Pedersen, Phys. Rev. B 47 (1993) 657.
[67] P.C. Aben, J. Catal. 10 (1968) 224.
[68] T.B. Flanagan, R. Balasubramaniam, R. Kirchheim, Platinum Metals Rev. 45 (2001) 114.
[69] N.K. Nag, J. Phys. Chem. B 105 (2001) 5945.
[70] M. Bonarowska, J. Pielaszek, W. Juszczyk, Z. Karpinski, J. Catal. 195 (2000) 304.
[71] E.W. Shin, S.I. Cho, J.H. Kang, W.J. Kim, J.D. Park, S.H. Moon, Korean J. Chem. Eng. 17 (2000) 468.

[72] N. Krishnankutty, J. Li, M.A. Vannice, Appl. Catal. A: Gen. 173 (1998) 137.
[73] F. Pinna, M. Signoretto, G. Strukul, S. Polizzi, N. Pernicone, React. Kinet. Catal. Lett. 60 (1997) 9.
[74] A.L. Bonivardi, M.A. Baltanas, J. Catal. 138 (1992) 500.
[75] F.A. Lewis, Platinum Metals Rev. 4 (1960) 132.
[76] G. Fagherazzi, A. Benedetti, S. Polizzi, A. Mario, F. Pinna, M. Signoretto, N. Pernicone, Catal. Lett. 32 (1995) 293.
[77] X.P. Xu, D.W. Goodman, J. Phys. Chem. 97 (1993) 7711.
[78] X.P. Xu, P.J. Chen, D.W. Goodman, J. Phys. Chem. 98 (1994) 9242.
[79] V.E. Henrich, P.A. Cox, The Surface Science of Metal Oxides, Cambridge University Press, Cambridge, 1994.
[80] M.A. Barteau, Chem. Rev. 96 (1996) 1413.
[81] M.A. Barteau, J.M. Vohs, Oxide model systems, in: G. Ertl, H. Knözinger, J. Weitkamp (Eds.), Handbook of Heterogeneous Catalysis, vol. 2, Wiley-VCH, Weinheim, 1997.
[82] C. Xu, D.W. Goodman, Ultrathin oxide films: model catalyst supports, in: G. Ertl, H. Knözinger, J. Weitkamp (Eds.), Handbook of Heterogeneous Catalysis, vol. 2, Wiley-VCH, Weinheim, 1997.
[83] H.J. Freund, Angew. Chem. Int. Edit. Engl. 36 (1997) 452.
[84] K. Wolter, O. Seiferth, J. Libuda, H. Kuhlenbeck, M. Baumer, H.J. Freund, Chem. Phys. Lett. 277 (1997) 513.
[85] K. Wolter, O. Seiferth, J. Libuda, H. Kuhlenbeck, M. Baumer, H.J. Freund, Surf. Sci. 404 (1998) 428.
[86] K. Wolter, O. Seiferth, H. Kuhlenbeck, M. Bäumer, H.J. Freund, Surf. Sci. 399 (1998) 190.
[87] C.R. Henry, Surf. Sci. Rep. 31 (1998) 235.
[88] S. Surnev, M. Sock, M.G. Ramsey, F.P. Netzer, M. Wiklund, M. Borg, J.N. Andersen, Surf. Sci. 470 (2000) 171.
[89] H.J. Freund, M. Baumer, H. Kuhlenbeck, Adv. Catal. 45 (2000) 333.
[90] N. Sheppard, C. De La Cruz, Catal. Today 70 (2001) 3.
[91] E. Ozensoy, D.W. Goodman, Phys. Chem. Chem. Phys. 6 (2004) 3765.
[92] J.S. Bradley, E.W. Hill, S. Behal, C. Klein, B. Chaudret, A. Duteil, Chem. Mater. 4 (1992) 1234.
[93] J.S. Bradley, J.M. Millar, E.W. Hill, S. Behal, J. Catal. 129 (1991) 530.
[94] L.L. Sheu, Z. Karpinski, W.M.H. Sachtler, J. Phys. Chem. 93 (1989) 4890.
[95] L.-L. Sheu, H. Knozinger, W.M.H. Sachtler, J. Am. Chem. Soc. 111 (1989) 8125.